DOI 10.1007/s11015-019-00739-5

Metallurgist, Vol. 62, Nos. 9-10, January, 2019 (Russian Original Nos. 9-10, September–October, 2018)

QUANTITATIVE ANALYSIS OF CARBIDE PHASES IN MEDIUM-CARBON STEEL AFTER LOW-TEMPERATURE TEMPERING

V. V. Ryabov,[1,2] **E. I. Khlusova,**[1] **A. A. Zisman,**[1] **S. V. Rogozhkin,**[3,4] **A. A. Nikitin,**[3,4] **and A. A. Luk'yanchuk**[3]

UDC 669.14.018.295:625.785.6

Structural features of high-strength wear-resistant steel formed after tempering at different temperatures are investigated. Temperature dependences are determined for steel hardness and impact strength. Temperature ranges are recorded for intermediate carbide formation, cementite particle formation, and residual austenite decomposition. The lath structure and carbide particle distribution are analyzed using transmission electron microscopy. Neutron diffraction is used to study the dependence of the proportion of retained austenite on temperature. Atom probe tomography is used to analyze micro-inhomogeneity in carbon and alloying element distribution.

Keywords: medium carbon steels, carbides, martensite, neutron diffraction, atom probe tomography.

Work for studying the effect of alloying elements on the structure and properties of medium-carbon steels with a martensitic structure after quenching and low-temperature tempering has been conducted since the 1960–1970s [1–4]. In view of the increasing requirement for high-strength and wear-resistant steels in the last decade this work has also been carried out overseas [5, 6]. Development of contemporary research equipment, expansion of the procedural bases of experiments, make it possible to use a comprehensive approach in studying features of steel structure and property formation [7–9]. Methods are used in this work of differential dilatometry, transmission electron microscopy (TEM), and in addition to these the method of atom probe tomography making it possible on an atomic scale to analyze chemical element distribution in test steels. In combination with data for determining mechanical properties and hardness measurement of a new medium-carbon steel correlation is discussed in the work of structural features and production regimes for steel heat treatment. It has been shown in [10–14] that with low temperature tempering nanosize particles of intermediate carbides are formed, increasing material wear resistance and strength with retention of a satisfactory level of ductility and toughness.

The aim of the work is comprehensive quantitative analysis of carbon and alloying element distribution in a new medium-carbon wear-resistant steel B1700 after tempering and determination of the effect of chemical inhomogeneity on a nanometric scale on its toughness and ductility.

Research Material and Procedure

High-strength wear-resistant steel B1700 [15] was studied, developed for manufacturing components of soil cultivation engineering, of the following chemical composition (ladle sample), wt.% C 0.45, Si 0.36, Mn 1.13,

[1] NITs Kurchatov Institute – TsNII KM Prometei, St. Petersburg, Russia.

[2] E-mail: viacheslav_riabov@crism.ru.

[3] NITs Kurchatov Institute – ITÉF, Moscow, Russia.

[4] National Research Nuclear University MIFI, Moscow, Russia.

Translated from Metallurg, Vol. 62, No. 9, pp. 64–70, September, 2018. Original article submitted January 29, 2018.

 0026-0894/19/0910-0926

Table 1
Specimen Heat Treatment Regime and Marking

Specimen number	Heat treatment regime
1	Oil quenching 900 °C, 1.5 h, tempering 350 °C, 4 h
2	Oil quenching 900 °C, 1.5 h, tempering 150 °C, 4 h

Table 2
Test Specimen Mechanical Properties after Treatment

Specimen number	$\sigma_{0.2}$, MPa	σ_f, MPa	δ_5, %	δ_p, %	ψ, %	KCU^{+20}, J/cm^2	*HRC*
1	1445	1695	7.1	2.7	10.5	36	47.6
2	1655	1985	10.3	2.8	21.0	55	52.1

Ni 0.67, Cu 0.63, Cr 1.26, Mo 0.40, Ti 0.03, V 0.06, Nb 0.02, Al 0.04, Ca (by calculation) 0.03, B (by calculation) 0.003, S 0.008, P 0.005.

Rolled sheet 6 mm thick was prepared from 40 kg ingots melted in an induction furnace. Ingots were forged in a hammer with dropping weight of 3000 kg. Forging were rolled in DUO-600 reversing mill in the range 1100–900 °C after heating in a chamber furnace to 1200 °C. Quenching and low-temperature tempering were performed in laboratory chamber furnaces. Heat treatment (HT) and mechanical properties of specimens are given in Tables 1 and 2 respectively. Tensile and impact bending tests were performed in accordance with the specifications of GOST 1497 and GOST 9454. Hardness measurement was carried out in a Rockwell hardness meter according to GOST 9013.

Foils for TEM were prepared by electrolytic thinning followed by cleaning in a Fischione 1910 Ion Mill ion etching unit. A study of material fine structure was performed by means of an FEI Technai G^2 30 S-TWIN transmission electron microscope with an accelerating voltage of 200 kV. Dislocation density was determined by the intersection method. Residual austenite and carbide phase content were studied by a neutron diffraction method using a SKAT diffractometer [16] in a pulsed IBR-2 (OIYaI, Dubna) reactor. Analysis of carbon and alloying element distribution micro-inhomogeneity was carried out by atom probe tomography in a PAZA-3D (ITEF) [17] unit according to the procedure in [18]; needle specimens were prepared by means of electrochemical polishing.

Effect of Tempering Temperature on Steel Hardness and Impact Strength

Results are given in Fig. 1 for determining steel impact strength and hardness in relation to tempering temperature. After tempering at 150–350 °C no significant reduction is observed in hardness compared with the quenched condition, hardness above 40 HRC is retained up to 800 °C, and after tempering at higher temperature hardness decreases to 28 HRC.

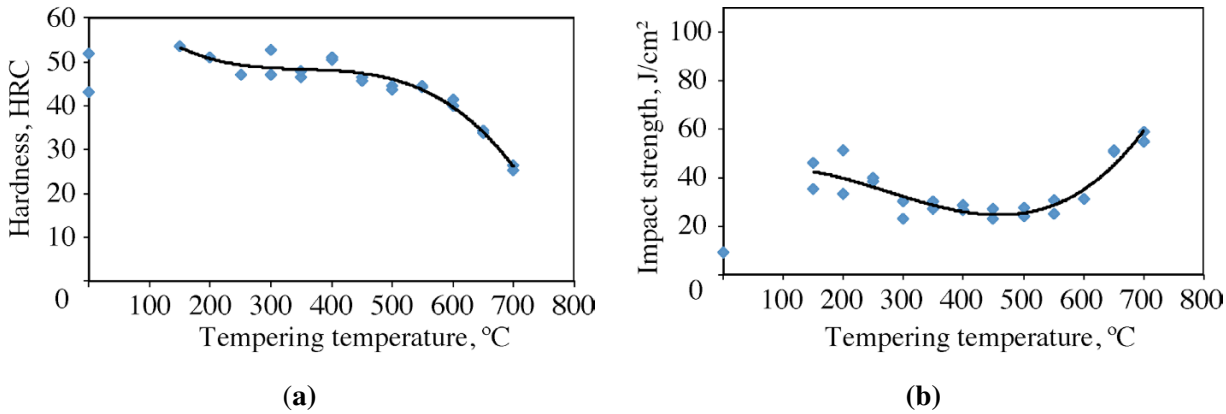

Fig. 1. Effect of tempering temperature on impact strength (a) and hardness (b) of steel B1700 [19].

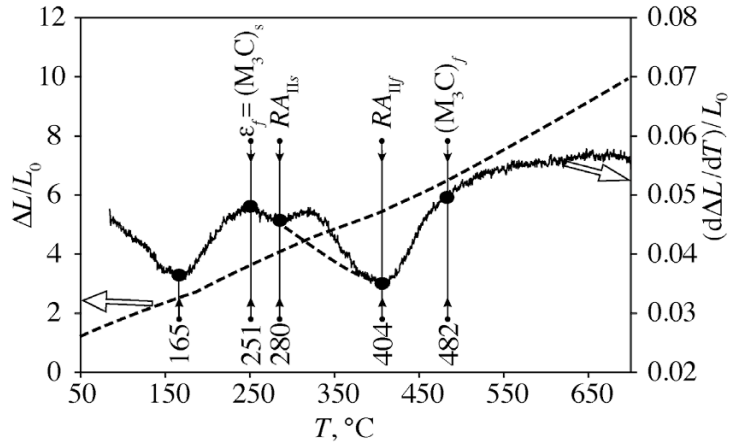

Fig. 2. Differential dilatometric curve for steel B1700 --- is original dilatometric curve; —— is differential curve; ε_f is finish of intermediate carbide formation; $(M_3C)_s$ and $(M_3C)_f$ are start and finish of cementite formation respectively; RA_{IIs} and RA_{IIf} are start and finish of residual austenite decomposition respectively.

In a quenched condition values of impact strength KCU^{+20} ate at a minimum and comprise about 10 J/cm^2. After low-temperature tempering at 150–250 °C impact strength increases to 35–55 J/cm^2 compared with the quenched condition, but with 300–600 °C a reduction is observed to 21–25 J/cm^2, which is apparently connected with development of temper brittleness of the first order. In medium-carbon steels the range of temper brittleness is within the limits of 250–400 °C, although in the test steel the broader temperature range for temper brittleness is due to the higher level of alloying having an effect on residual austenite decomposition and carbide formation processes. After high-temperature tempering at 650–700 °C an increase in impact strength is observed to 52–60 J/cm^2.

Results of Differential Dilatometry

In order to analyze structural transformations during specimen tempering after quenching from 900 °C they were heated in a vacuum chamber of a dilatometer to 700 °C at a rate of 0.05 °C/sec followed by cooling to room temperature at a rate of 50 °C/sec (Fig. 2, where ΔL is specimen change in length, L_0 is its original length).

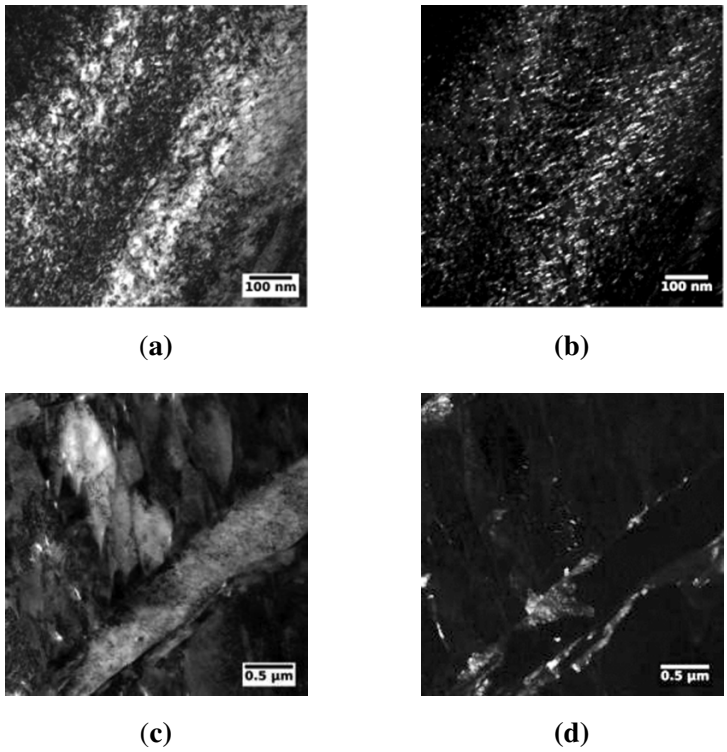

Fig. 3. Carbide phase distribution in steel B1700 after tempering: (a), (b) at 150 ºC; (c), (d) at 300 ºC; (a), (c) in light field; (b), (d) in dark field.

In order to analyze transformations during tempering from data for construction of the original dilatometric curve, a differential curve was plotted $(d\Delta L/dT)L_0$ reflecting the nature of transformation during heating with steel tempering (see Fig. 2). In particular, it is possible by this method to determine the temperature for the end of ε-carbide precipitation and also the temperature range for formation of cementite and residual austenite decomposition [8, 11, 14].

Results of analyzing the differential curve make it possible to propose that formation of E-carbide in the test steel commences at about 150 ºC. Presence of a minimum on this curve at 165 ºC may be explained by carbide formation. The region for interlath cementite precipitation and residual austenite decomposition is in the range 250–480 ºC.

Research Results in a Transmission Electron Microscope

A study of steel structure by TEM has shown [14] that after tempering at 1500 and 300 ºC the main steel structural component is martensite of three morphological types and lath martensite occupies 80–85% of a foil area. After tempering at 150 ºC and subsequent air cooling carbides from mainly in lamellar martensite (Fig. 3a, b). The volumetric density of dispersed particles comprises $220 \cdot 10^{20}$ m^{-3}.

An increase in tempering temperature to 300 ºC leads to nonuniform carbide formation within martensite of different morphology. In lamellar martensite the size of carbides increases to 147 nm, and their density is reduced to $1.5 \cdot 10^{20}$ m^{-3} (Fig. 3c, d). Within laths of lath martensite dispersed carbide density comprises $13 \cdot 10^{20}$ m^{-3} and particles of greater size (164 nm) are arranged over lath boundaries. At the boundaries of original austenite grains carbides are observed with a size up to 180 nm, and also residual austenite in an amount

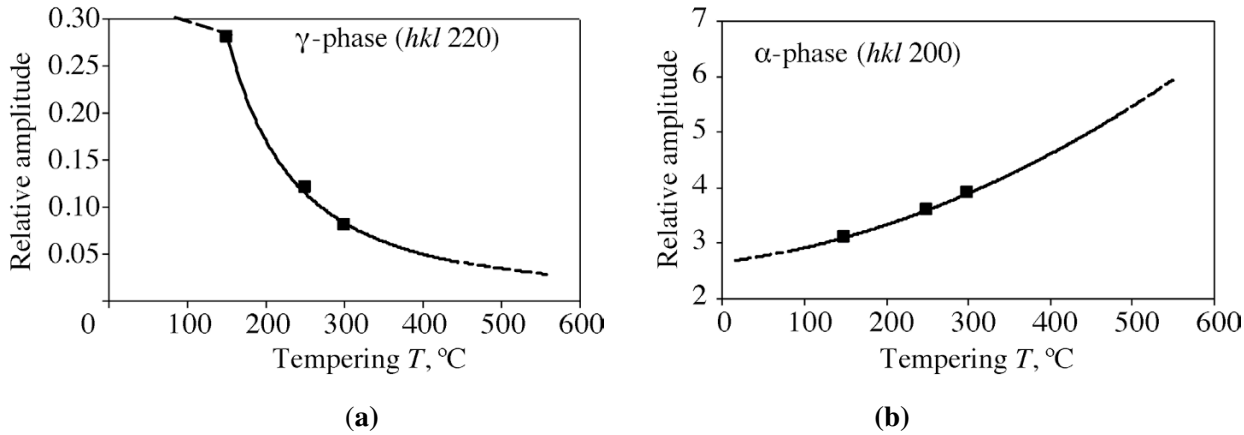

Fig. 4. Temperature dependence of relative amplitude of residual austenite diffraction peaks (a), α -phase (b) on steel B1700 tempering temperature.

Table 3
Steel B1700 Structure Parameters after Tempering at 150 and 300 °C [14]

Structure Parameters	Tempering at *T*, °C	
	150	300
Lath martensite, volume fraction, %	*80–85*	
Particles within laths:		
size, nm	–	26–164
bulk density $X10^{20}$ m^{-3}	–	13
Carbides at lath boundaries with length, nm	–	164
Lamellar martensite, volume fraction, %	*10–12*	
Particles within plates		
size, nm	13	147
bulk density $X10^{20}$ m^{-3}	220	1.5
Twinned martensite, volume fraction, %	*10–15*	
Residual austenite, volume fraction, not more than %	5	5
Carbides at original austenite grain boundaries, nm	–	180

of up to 5 vol.% (Table 3). After tempering at 150 °C carbides over austenite grain boundaries and between martensite laths are not revealed, but after tempering at 300 °C presence of coarse carbides with a size up to 180 nm points to decomposition of residual austenite with subsequent transformation into a ferrite-carbide mixture.

In performing *research by the neutron diffraction method* for recoding diffraction signals a "time of flight" experimental scheme was used for recording signals [16]: radiation is characterized by a broad continuous wavelength λ range, and the diffraction angle θ is recorded. Therefore, in contrast to a standard scheme, under Wolfe–Bragg conditions: $2d \sin\theta = \lambda$ varies not in diffraction angle θ, but wavelength λ, and different

Table 4
Chemical Composition of Steel B1700 Specimen after Tempering at 150 °C (at.%)

Composition determination location	C	Si	Mn	Ni	Cu	Cr	Mo	Ti	V	Nb	Al
For ladle sample	0.45	0.36	1.13	0.67	0.63	1.26	0.40	0.03	0.06	0.02	0.04
Middle through volume	0.64	0.42	1.11	0.49	0.62	1.37	0.23	–	0.07	0.10	0.04
Matrix without considering cluster/segregations	0.26	0.41	1.09	0.38	0.46	1.34	0.19	–	0.07	0.05	0.05
Region 1	0.97	0.53	1.31	0.49	0.51	1.54	0.32	–	0.08	0.12	0.09
Region 2	0.71	0.28	1.13	0.94	1.05	1.34	0.38	–	0.07	0.32	0.04

values of λ concern narrow channels of in which with respect to time of flight the horizontal axis of diffraction spectra is broken down.

The dependence of relative amplitude is shown in Fig. 4a (I/I_b, where I is diffraction peak amplitude, I_b is local background amplitude) of diffraction peak (220) γ for residual austenite on tempering temperature for steel B1700. A similar dependence for α-phase (martensite) is shown in Fig. 4b).

These results point to a gradual reduction in the proportion of residual austenite (see Fig. 4a) with an increase in the proportion of α-phase (se Fig. 4b) with an increase in specimen tempering temperature from 150 to 300 °C. As is well known, in austenite increased carbon solubility and austenite decomposition lead to carbide precipitation. This is confirmed by an increase in relative amplitude of diffraction peaks (200) for α in Fig. 4b.

Results of Atom Probe Tomography. Tempering at 150 °C.

Specimens of rolled sheet after tempering at different temperatures were also analyzed using atom probe tomography for studying carbon and main alloying element distribution. The chemical composition of a specimen after tempering at 150 °C is given in Table 4.

Presence of distinct peaks for cementite (Fe_3C) were only revealed with a tempering temperature of 550 °C (Fig. 5), and only with a tempering temperature above 350 °C.

Chemical composition of the matrix without considering clusters corresponds approximately to the average for volume concentration of alloying elements and is similar to the steel chemical composition, with the exception of carbon, nickel, molybdenum, and niobium content. The matrix is impoverished with respect to carbon, which to all appearances points to presence of regions of intermediate Caribe separation, forming clusters. Atom maps are given in Fig. 6 for a specimen after tempering at 150 °C in studying a region with a size of $23 \times 23 \times 200$ nm^3.

A concentration profile (Fig. 7) was plotted in order to analyze the distribution of atoms in a microprobe section. Analysis of atomic maps makes it possible to record different carbon and alloying element distribution in test specimens after tempering at 150 and 350 °C.

After specimen tempering at 150 °C the carbon distribution along a region studied of 110 nm in length is characterized by several segregations, where its average concentration comprises about 1.5 at.%. The greatest carbon segregation correlates (for location) with segregation of nickel, niobium, and molybdenum. Attention

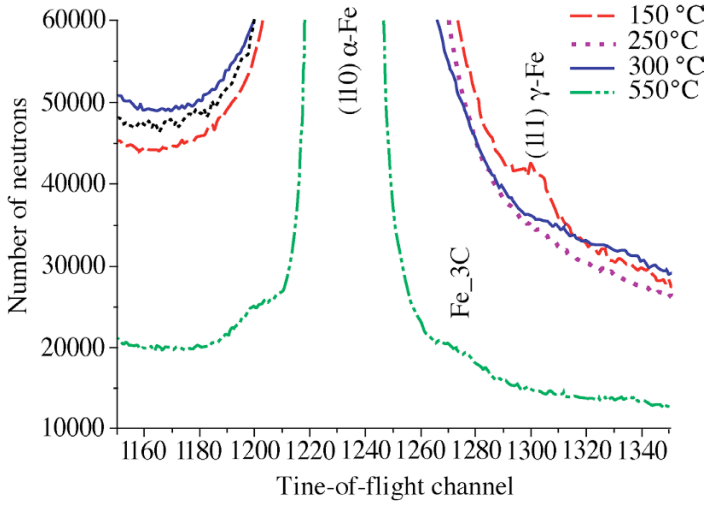

Fig. 5. Diffraction peak for cementite (Fe_3C) in study by neutron diffraction method.

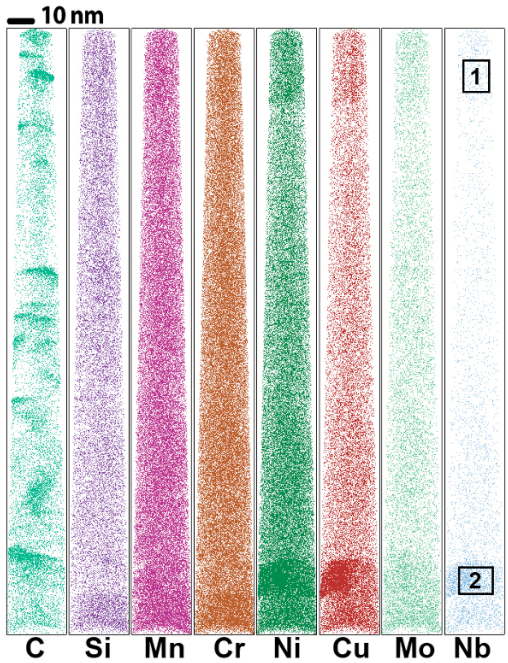

Fig. 6. Atomic map of specimen after tempering at 150 °C; figures 1 and 2 indicate regions separated for analysis of local chemical composition (see Table 4).

is drawn to the fact that migration mobility of nickel at 150 °C is insignificant, and it may be suggested that this correlation points to layering of residual austenite, in which an increased nickel content is inherited from the original structure. Since the carbon diffusion coefficient in austenite is an order of magnitude higher than in martensite, but the scale of the region studied is comparable with the thickness of martensite oaths, it is entirely probable that the martensite layer in question is located at a boundary between laths, and region 2 (see Fig. 6) probably corresponds to previous niobium carbide and/or alloyed cementite.

The spatial distribution of carbon atoms and main alloying elements after tempering at 350 °C is presented in Fig. 8 in the form of atomic maps. The size of a test region was $25 \times 25 \times 100$ nm^3. One coarse accumulation

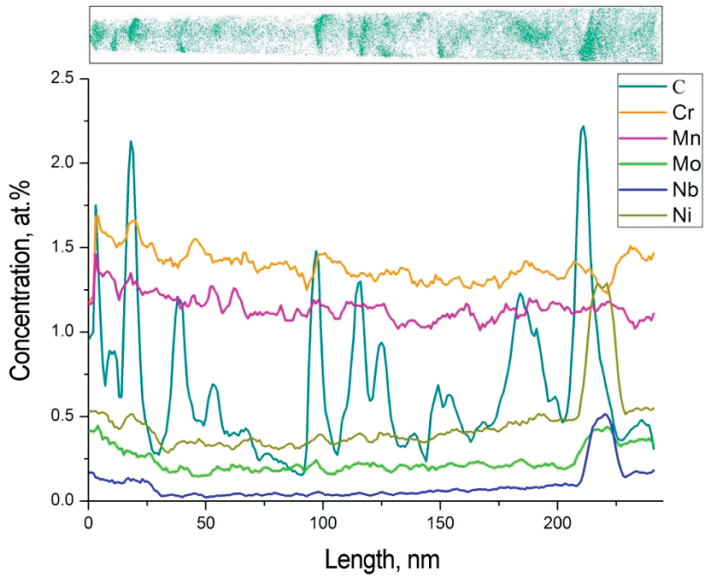

Fig. 7. Atomic map of carbon and concentration profile for other elements along test specimen axis after tempering at 150 ºC.

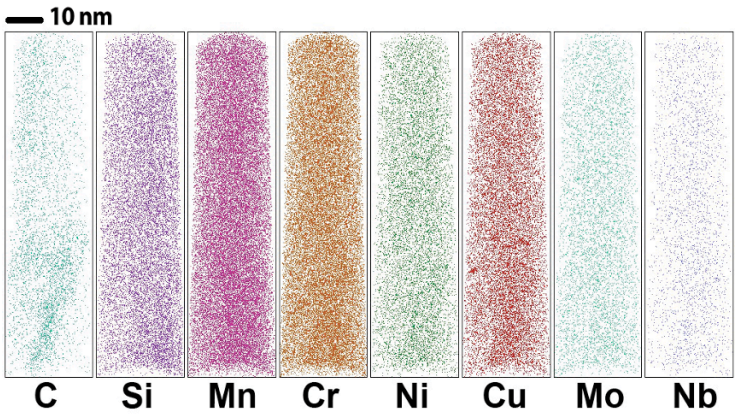

Fig. 8. Atomic map of specimen after tempering at 350 ºC.

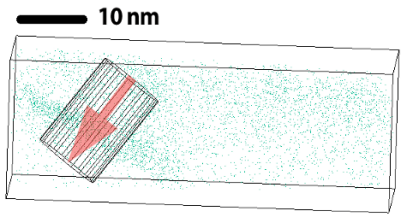

Fig. 9. Atomic map of carbon distribution close to previously detected local features (see Fig. 8).

of carbon atoms is observed within it, which may specify a region of previous cementite type carbide, alloyed with chromium and molybdenum, at a boundary between martensite laths. The distribution of alloying element atoms with intersection of this accumulation (Fig. 9) is presented in Fig. 10.

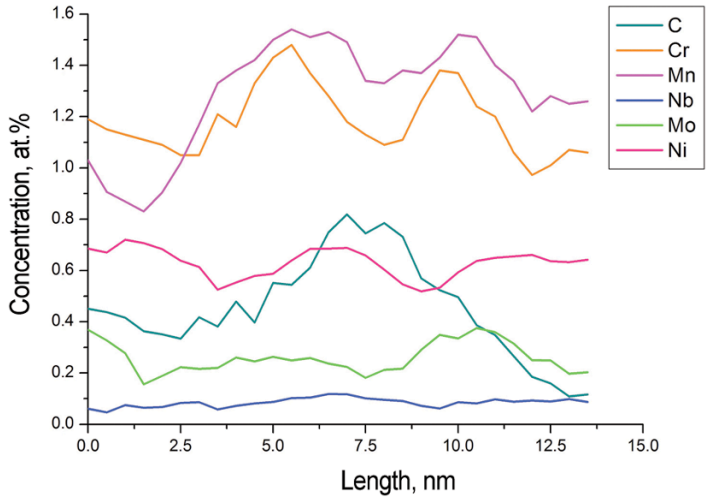

Fig. 10. Concentration profile along direction indicated by arrow in Fig. 9.

Table 5
Specimen Chemical Composition after Tempering at 350 °C (at.%)

Composition determination location	C	Si	Mn	Ni	Cu	Cr	Mo	Ti	V	Nb	Al
For ladle sample	0.45	0.36	1.13	0.67	0.63	1.26	0.40	0.03	0.06	0.02	0.040
Middle through volume	0.37	0.41	1.16	0.61	0.57	1.37	0.23	–	0.07	0.10	0.05
Matrix without considering cluster/segregations	0.37	0.40	1.14	0.60	0.55	1.35	0.22	–	0.07	0.10	0.05

The average chemical composition of the test region is given in Table 5. Matrix composition without taking account of clusters corresponds approximately to the average volume concentration of alloying elements and is close to the steel composition with the exception of carbon, molybdenum, and niobium.

In a concentration profile (see Fig. 10) in a direction indicated in Fig. 9 a suggested boundary is observed for carbon enrichment (up to 0.8 at.%), and also with respect to chromium and manganese (up to 1.5 at. % each). In addition, close to the boundary some enrichment is observed with respect to molybdenum (up to 0.3 at > %). At the same time niobium atoms are distributed almost uniformly.

Therefore, comprehensive analysis of steels B1700 structure after low-temperature tempering has shown that good viscoplastic properties (relative reduction of area, relative elongation, and impact strength) combined with high hardness are observed after tempering at 150 °C when there is layering with respect to carbon, cluster formation, and also preprecipitated and intermediate carbides predominantly within lamellar martensite. An increase in tempering temperature to 300–350 °C facilitates breakdown of residual austenite regions, formation cementite type carbide, alloyed with chromium, manganese, and molybdenum, over lath boundaries and the boundaries of previous austenite grains, which leads to a reduction in ductility and toughness by a factor of 1.5–2 and also steel hardness.

Conclusions

1. A study of the effect of temperature on hardness and impact strength of a new high-strength wear-resistant steel B1700 has shown that the highest hardness values are achieved after tempering at 150–250 °C, and impact strength has a satisfactory value of 35–55 J/cm^2 combined with good ductility properties. Tempering at 350 °C leads to a reduction in impact strength to 21–25 J/cm^2, and for relative reduction of area and relative elongation by a factor of 1.5–2.

2. The main structural component (80–85%) of steel B1700 is lath martensite, also revealed as lamellar martensite with a volume fraction of 10–12%, and twinned martensite (10–15%). Analysis of carbide formation processes conducted by differential dilatometry showed that at 150 °C there is formation of a new intermediate type carbides, and at 250–480 °C there is austenite decomposition with simultaneous separation of interlath martensite. The neutron diffraction method showed a reduction in the proportion of residual austenite with a simultaneous increase in the proportion of α-phase with an increase in temperature from 150 to 300 °C; a diffraction peak for cementite is revealed in a specimen after tempering at 550 °C.

3. Studies by atom probe microscopy made it possible to reveal numerous accumulations of carbon atoms in a specimen after tempering at 150 °C, suggesting characteristic preprecipitation of intermediate carbides and a coarse accumulation of atoms of carbon, chromium, manganese, and molybdenum in a specimen after tempering at 350 °C, which makes it possible specify it as alloyed cementite. The data obtained are in good agreement with data of transmission electron microscopy: after tempering at 150 °C the finest carbides were observed with an average size of 13 nm and volumetric density of $220 \cdot 10^{20}$ m^{-3}, recorded predominantly in lamellar martensite. An increase in tempering temperature to 300 °C leads to nonuniform carbide formation in martensite of different morphology: coarse particles have been observed with size up to 164–180 nm at lath martensite boundaries and at boundaries of original austenite grains, where residual austenite with volume fraction up to 5% is also encountered.

Therefore, combined use of research methods, i.e., transmission electron microscopy, differential dilatometry, neutron diffraction, and atom probe tomography, make it possible to record quantitatively transformation processes during tempering in medium-carbon steel, and to evaluate the effect of chemical inhomogeneity on strength, toughness, and ductility of steel in order to select the most suitable tempering regimes.

Experimental research was carried on equipment of the Center for Collective Usage for Scientific Equipment “Composition, structure and properties of structural materials NITs Kurchatov Institute – TsNII KM Prometei with financial support of the state in the name of the Ministry of Education and Science within the scope of an agreement No. 14.595.21.0004, unique identifier RFMEF159517X0004. Tomographic atom probe analysis was conducted on equipment of the KAMIKS (http://kamiks.itep.ru/) NITs Kurchatov Institute – ITÉF.

REFERENCES

1. R. G. Baker and J. Nutting, “The tempering of 2.25Cr–lMo steel after quenching and normalizing,” *J. Iron and Steel Institute*, No. 192, 257–268 (1959).
2. Y. Hirotsu and S. Nagakura, “Crystal structure and morphology of the carbide precipitated from martensitic high carbon steel during the first stage of tempering,” *Acta Metallurgica*, No. 20, 645–648 (1972).

3. Y. Hirotsu, S. Nagakura, and S. Okuteni, "The crystal structure and morphology of the precipitated of the first stage of tempering of a high carbon 1.13 wt. % steel," Proc. of the Int. Conf. "Science and Technology of Iron and Steel," ICSTIS (1971).
4. D L. Wiliamson, K. Nakazawa, and G. Krauss, "A study of the early stages of tempering in an Fe-1.2 % alloy," *Metallurgical Trans. A*, No. 10, 1351–1355 (1979).
5. G. Zajac and J. Pacyna, "The kinetics of phase transformation during tempering in structural steels with nickel," *Proc. of 13th Int. Sci. Conf. on Achievements in Mechanical and Materials Engineering*, Gliwice, Wisla (2005).
6. J. Pacyna, "Dilatometric investigations of phase transformations at heating and cooling of hardened, unalloyed, high-carbon steel," *J. of Achievements in Materials and Manufacturing Engineering*, No. 46, 7–17 (2011).
7. Z. Kędzierski, *Phase Transformations in Metals and Alloys*, AGH University of Science and Technology (1988).
8. J. Pacyna and B. Pawlowski, "Effect of tempering temperature on 30HGSA steel toughness," *Metallurgy and Casting*, No. 10, 409–421 (1984).
9. V. M. Salganik, P. P. Poletskov, M. S. Gushchina, et al., " Features of obtaining nano-structured rolled sheet," *Vest. Gomel. Gos. Tekhn. Univ., im P. O. Sukhogo*, **1**, No. 1(60), 27–30 (2015).
10. V. V. Rybin, A. S. Rubtsov, and E. V. Nesterov, "Single reflection method and its application for electron-microscope analysis of dispersed phases," *Zavod. Lab.,* No. 8, 21–26 (1982).
11. V. V. Ryabov, E. I. Khlusova, S. A. Golosienko, and G. D. Motovilina, "New steels for agricultural engineering," *Metallurg,* No. 6, 59–65 (2015).
12. E. M. Grinberg and A. A. Alekseev, "X-ray phase study of low-temperature decomposition of hardened medium-carbon steel martensite," *Vopros. Materialoved.*, No. 3(83), 26–29 (2015).
13. A. A. Alekseev and E. M. Grinberg, "Effect of cooling rate during hardening on low-temperature kinetics for low-carbon steel martensite transformation," *Fiz. Metal. Metalloved.*, **115**, No. 10, 1086–1089 (2014).
14. V. V. Ryabov, T. V. Knyazyuk, M. S. Mikhailov, et al., "Structure and properties of new wear-resistant steel for agricultural engineering," *Vopros. Materialoved.*, No. 2(86), 7–19 (2016).
15. E. I. Khlusova, S. A. Golosienko, V. V. Ryabov, et al., RF Patent 2606825, MPK C22C38/54. High-strength wear-resistant steel for agricultural machines (Versions), Patent holder FGUP TsNII KM Prometei, No. 2015125002, 06.24.2015.
16. T. Lychagina, A. Zisman, E. Yashina, and D. Nikolayev, "Directly verifiable neutron diffraction technique to determine retained austenite in steel," *Advanced Engineering Materials*, 1700559 (2017). doi:10.1002/adem.201700559
17. S. V. Rogozhkin, A. A. Aleev, A. S. Shugov, et. al., "Atomic probe prototype with laser evaporation," *Pribory Tekhnika Éksperimenta*, No. 3, 129–134 (2017).
18. O. A. Reznitsyn, A. A. Luk'yanchuk, A. S. Shutov, et al., "Optimization of material analysis parameters by atomic probe tomography methods with laser evaporation of atoms," *Mass-Spektrometriya*, **14**, No. 1, 33–39 (2017).
19. E. I. Khlusova, G. D. Motovilina, and Yu. V. Linova, "Effect of tempering on the structure and the mechanical properties of rolled product of new high-strength medium-alloy steel for agricultural engineering," *Proizvod. Prokata*, No. 11, 41–48 (2016).